JOURNAL OF THERMOPHYSICS AND HEAT TRANSFER
Vol. 19, No. 4, October–December 2005

Heat Transfer on Flat Surface Impinged by an Underexpanded Sonic Jet

Man Sun Yu*
Yonsei University, Seoul 120-749, Republic of Korea
Byung Gi Kim†
LG Cable Ltd., Anyang 135-090, Republic of Korea
and
Hyung Hee Cho‡
Yonsei University, Seoul 120-749, Republic of Korea

Underexpanded impinging jets include complicated flow phenomena such as shock structure, sonic surface, and recirculation zone in a central impingement region, and the local heat transfer on an impinged surface has a different characteristic than a subsonic impinging jet. Studying this can be helpful in understanding the relation between supersonic flow characteristics and heat transfer on a surface. It can also provide a proper design factor for the impingement cooling technique by a high-speed jet. The convective heat transfer coefficients have been measured on a flat surface impinged by an underexpanded sonic jet. In addition, the visualization of shock structures and surface pressure measurements have been conducted to support the heat transfer measurement results. From the results, the distribution of the heat transfer coefficient on the central impingement region due to the interaction between the sonic surface and recirculation flow has been obtained. It has also been observed that the turbulence diffusion from the shear layers around the jet edge and the sonic surface into a jet core induce high heat transfer on a surface.

Nomenclature

A_f	=	area of the heated surface
B_{NE}	=	exit height of a slot nozzle
D_{NE}	=	exit diameter of a circular nozzle
h	=	convective heat transfer coefficient
I	=	electric current passing through heated foil
k_a	=	thermal conductivity of air
M_D	=	design Mach number at the nozzle exit
Nu	=	Nusselt number
P_a	=	ambient pressure
P_e	=	pressure at the nozzle exit plane
P_0	=	pressure in settling chamber
q	=	net heat flux generated from a heated foil to a jet flow
q_l	=	heat flux loss by conduction to the back of the test plate and radiation
q_q	=	total heat flux generated from a heated foil
R	=	radial distance from the stagnation point on an impinging surface
R_s	=	electrical resistance of shunt
T_{AW}	=	adiabatic wall temperature
T_w	=	wall temperature under the constant heat flux condition
V_f	=	voltage drop across the heated foil
V_s	=	voltage drop across the shunt
Z_{IE}	=	initial expansion length
Z_P	=	nozzle-to-plate distance
γ	=	specific heat ratio

Presented as Paper 2004-490 at the AIAA 42nd Aerospace Sciences Meeting and Exhibit, Reno, NV, 5–8 January 2004; received 30 October 2004; revision received 12 February 2005; accepted for publication 14 February 2005.

*Graduate Student, Department of Mechanical Engineering, Sinchon-dong 134, Seodaemun-gu; msyoo@yonsei.ac.kr. Member AIAA.
†Assistant General Manager, Hogae-dong 555, Dongan-gu.
‡Professor, Department of Mechanical Engineering, Shinchon-dong 134, Seodaemun-gu; hhcho@yonsei.ac.kr. Member AIAA.

I. Introduction

IF a jet issuing from a nozzle impinges on a surface, the surface is cooled or heated by thermal convection. For several decades, many studies have been conducted to understand this heat transfer phenomenon and find the optimum design factors for the best jet impingement effect. However, these studies have been focused mainly on subsonic jet impingement, but few on supersonic jets.

For a subsonic impinging jet, the studies on a heat transfer were summarized by Jambunathan et al.,[1] who reported that turbulent flow can affect heat transfer improvement on the impinged surface, as well as flow transport speed, that is, jet velocity. In particular, Gardon and Akfirat[2] and Gardon and Cobonpue[3] observed that turbulence diffusion from a jet edge into the core induces high heat transfer on a surface. They also found that the transition from laminar to turbulent wall jet flow on a surface can increase heat transfer, as in the case of flow separation by the secondary vortex movement. In addition, Gardon and Cobonpue[3] reported that the high wall jet speed leads to high heat transfer on a specific radial position ($R/D_{\mathrm{NE}} \approx \pm 0.5$) for nozzle-to-plate distances shorter than $Z_P/D_{\mathrm{NE}} = 6$. Decades later, Pamadi and Belov[4] also tried to explain this phenomenon with the effect of turbulence developed around an edge of freejet flow.

When the impinging jet has a supersonic speed, the shock structure may appear in front of the impinged solid surface. This phenomenon can be found in several engineering applications such as an antiship missile launching against fire-proof walls, an impingement of combusted gas onto the surface of jet vane, the quenching of a steel ingot, etc. Although many studies were reported on the heat transfer on a surface by a subsonic jet, as mentioned in the preceding paragraph, studies on high-speed impinging jets with shock structure are mainly related to visualizing the shock structure and measuring the surface pressure distribution.[5–8] Also, several simulation studies on underexpanded impinging jets did not consider the heat transfer to the impinged surface.[9,10] Because the jet flow with shock structure is significantly different with a subsonic jet, it can be expected that the heat transfer phenomenon will also be largely different between these two kinds of impinging jets.

In this study, an investigation has been carried out to examine heat transfer characteristics of an underexpanded impinging sonic jet. Distributions of the heat transfer coefficient on a flat plate have been obtained in detail. To accomplish this, temperature distributions

have been measured under the constant heat flux condition on an impinged surface. The adiabatic wall temperature distributions have also been measured because the temperature loss due to the dynamic temperature can not be ignored, and the energy separation effect appears on a surface for a high-speed impinging jet. In addition, distributions of surface pressure have been measured, and the shock structures in the jet have been visualized using a shadowgraph method. From the experimental results, the heat transfer mechanism is explained. The following parameters of interest have been considered: One is the underexpansion ratio, which is defined by the ratio of the nozzle exit pressure to the ambient pressure, and the other is the nozzle-to-plate distance. The results of the present study provide basic information to aid in the understanding of unknown aspects of heat transfer mechanisms by underexpanded impinging jets. Also, these results provide a basic concept to aid in the design of an impingement cooling/heating method using high-speed jets.

II. Experimental Apparatus

Figure 1 shows a schematic of the experimental apparatus used in the present study. Compressed air passes through seven-stage air filters to remove moisture and dust. It is then stored in six storage tanks, whose total volume and pressure are 0.69 m^3 and 15.2 MPa, respectively. When the valve is opened, the air is depressurized using a regulator (Yamato sangyo, YR-5062) set to the design value and supplied to the settling chamber. In the settling chamber, the airflow is decelerated and becomes uniform for the measurement of total pressure and temperature. The convergent circular nozzle is attached to the settling chamber, and its exit diameter is 0.01 m. During the test, the air stagnation temperature decreases moderately due to a combination of the Joule–Thomson effect across valves and expansion effects in storage tanks, etc. To avoid this change of total air temperature, the supplied air was heated to the ambient temperature level with an electric heater between the storage tanks and the settling chamber. The electrical power supply to the heater was controlled automatically by a computer during the test. The temperature lag between the air in a settling chamber and the ambient air was measured to within 0.5°C.

The test plate for heat transfer measurement consists of the heating foil, the backing of insulated layers, and thermocouples. A stainless steel heating foil, whose thickness is 25.4×10^{-6} m, is bonded onto a 0.003-m thick Bakelite plate with a double-sided adhesive tape. The area of heated surface is 0.0354 m^2. When the electrical power is supplied, the heating foil provides a constant heat flux condition. To determine the electrical power supplied to the surface, the voltage drop across the heating foil is measured during a run. The electrical current is also obtained by measuring the voltage drop across a shunt, which is placed in the middle of the electrical circuit. The backside of the plate is insulated thermally with a paper honeycomb (air gap), fiberglass, and acrylic to reduce thermal loss. On the plate, 41 T-type thermocouple junctions are instrumented in a row, and their spacing is determined differently according to their positions: 0.0025 m between $-3 \le R/D_{NE} \le +3$ and 0.005 m in the outer region ($R/D_{NE} < -3$ or $3 < R/D_{NE}$).

Another plate is used for measurement of the surface pressure. It is made of 0.02-m-thick acrylic, and two pressure taps were drilled into the plate. One of them is positioned on the geometrical center point of the plate, and the other is 0.02 m away from it. These pressure taps are connected to the pressure transducer (Druck, PMP4070), and the plate is shifted laterally with spacing of 0.001 m during an experiment. This method can enable measurement of the pressure distribution on an impinged surface in a 0.04-m lateral region. As for the movement of the test plate, it is fixed to a linear motion system with two axes (Samik LMS, SAR1110T-200/400) driven by stepping motors (Oriental Motors, PK596NA). The stroke of the axial direction is 0.4 m and that of the lateral direction is 0.2 m.

The output voltage signals from thermocouples and pressure transducers are scanned and acquired using Agilent 34970A data acquisition/switch units and were processed on a personal computer for conversion to values of pressure and temperature.

To visualize the shock structure in the jet flow, a shadowgraph method is used. A conventional shadowgraph system with a continuous light source of 30 W and two 0.1-m-diam convex lenses was constructed. The optical image of the flowfield is taken using a digital camera (Nikon, Coolpix 900) at a shutter speed of 1/500 s.

III. Experimental Method and Data Reduction

In general, the following relation is used for calculation of the convective heat transfer coefficient on a surface where a compressible high-speed jet impinges[11]:

$$h = q/(T_w - T_{aw}) \tag{1}$$

In this study, experimental results obtained by Kim et al.[12] were used for adiabatic wall temperature distribution T_{AW} for the calculation. To obtain the other two values, that is, q and T_w in Eq. (1), the wall temperature distribution was measured under the constant heat flux condition. The temperature measurement was conducted for about 30 s after steady state was reached. In most cases, the steady state was reached after about 4 min from the regulator opening time. The total heat flux from the heating foil q_q has the same value, with the electric power applied to the foil. The net heat flux to the jet flow q can be calculated by extracting other heat losses from the total heat flux, as in the following equation:

$$q = q_q - q_l \cong q_q - (q_{cond} + q_{rad}) \tag{2}$$

The heat losses q_l are supposed to occur primarily by conduction to the back of the test plate and as radiation from the surface of

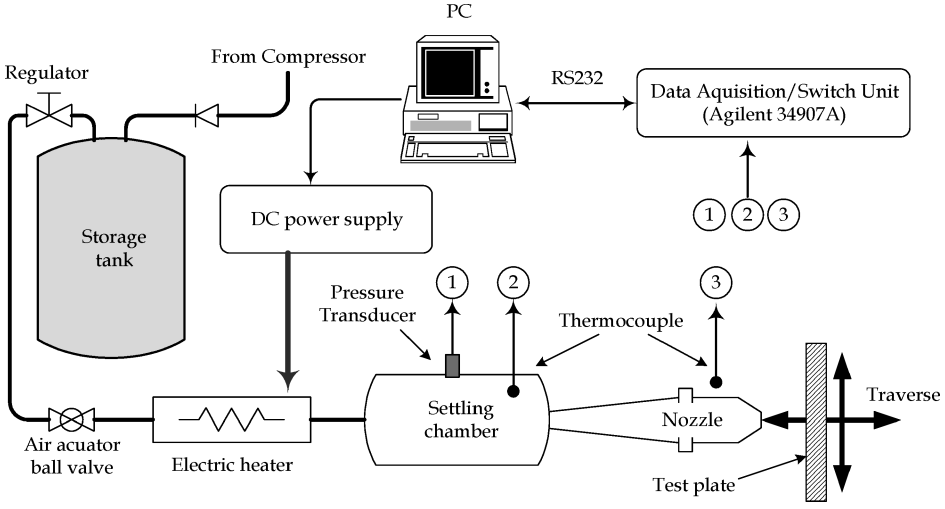

Fig. 1 Schematic of experimental apparatus.

heating foil. The maximum heat loss by thermal conduction was less than 0.1% of the total heat flux due to the good insulation of the test plate materials. The total thermal resistance of a test plate was calculated to about 1.04×10^4 m$^2 \cdot$ K/W. Heat loss due to radiation from the heating foil was calculated with the Stefan–Boltzmann law, and it was no more than 0.2% of the total heat flux. In the calculation, the emissivity of the heating foil (thin stainless steel foil) and the Stephan–Boltzmann constant were taken as 0.22 and 5.67×10^{-8} W/m$^2 \cdot$ K^4, respectively.

Finally, the local heat transfer coefficient was presented in terms of the Nusselt number as

$$Nu = hD_{\mathrm{NE}}/k_a \tag{3}$$

The experimental uncertainty is estimated using the method of Kline and McClintock[13] and Kline.[14] The uncertainty is calculated to be less than 7.0%, with a confidence level of 95%.

IV. Experimental Conditions

The underexpansion ratio is defined as the ratio of the nozzle exit pressure to the ambient pressure, P_e/P_a. In the test, the underexpansion ratio was considered to be from 1.5 to 3.5, and it corresponds to the nozzle pressure ratio (P_0/P_a) from 2.84 to 6.63. The nozzle pressure ratio is determined from the following relation:

$$P_0/P_a = (P_e/P_a)\left\{1 + [(\gamma - 1)/2]M_D^2\right\}^{\gamma/(\gamma-1)} \tag{4}$$

The nozzle-to-plate distance was varied in the range from one-half of a nozzle exit diameter to 20 diameters. The detailed measurements were conducted mainly at the small nozzle-to-plate distances.

V. Results and Discussion

A. Surface Pressure and Visualized Shock Structure

In the range of short nozzle-to-plate distances, the surface pressure on a center point shows a tendency to decrease with increasing distance.[12] For the sake of convenience, the nozzle-to-plate distance where the first minimum value of the central surface pressure appears is referred to as initial expansion length Z_{IE}. Figure 2 shows surface pressure profiles with various nozzle-to-plate distances for different underexpansion ratios. In the case of $P_e/P_a = 1.5$ (Fig. 2a), when the plate is placed at $Z_P/D_{\mathrm{NE}} = 0.5$, the surface pressure has a maximum at the center point and drops with increasing radial distance due to flow acceleration. This rapid fall in surface pressure in the central region is due to the expansion fan from the intersection of the standoff shock and the jet edge. After slight recompression at $R/D_{\mathrm{NE}} \approx 1.0$, the pressure approaches the ambient pressure ($P_a/P_0 = 0.35$). When the nozzle-to-plate distance increases to $Z_P/D_{\mathrm{NE}} = 1.0$, the pressure in the central region decreases. This decreased surface pressure is supposed to appear because total pressure loss across the central standoff shock becomes higher than in the case of $Z_P/D_{\mathrm{NE}} = 0.5$, due to the higher upstream Mach number. When the plate is placed at $Z_P/D_{\mathrm{NE}} = 1.2$, the maximum pressure occurs off center; the surface pressure has a maximum at $R/D_{\mathrm{NE}} \approx 0.4$. Such an annular maximum of the pressure suggests that recirculating flow, called a stagnation bubble, occurs in the central region as reported previously by other researchers.[6]

Shadowgraph images of an impinging jet for $P_e/P_a = 1.5$ are presented in Fig. 3a. In the smallest nozzle-to-plate distance ($Z_P/D_{\mathrm{NE}} = 0.5$), the standoff and reflected shocks are almost normal to the jet direction. As the nozzle-to-plate distance increases, the reflected shock becomes oblique, whereas the standoff shock

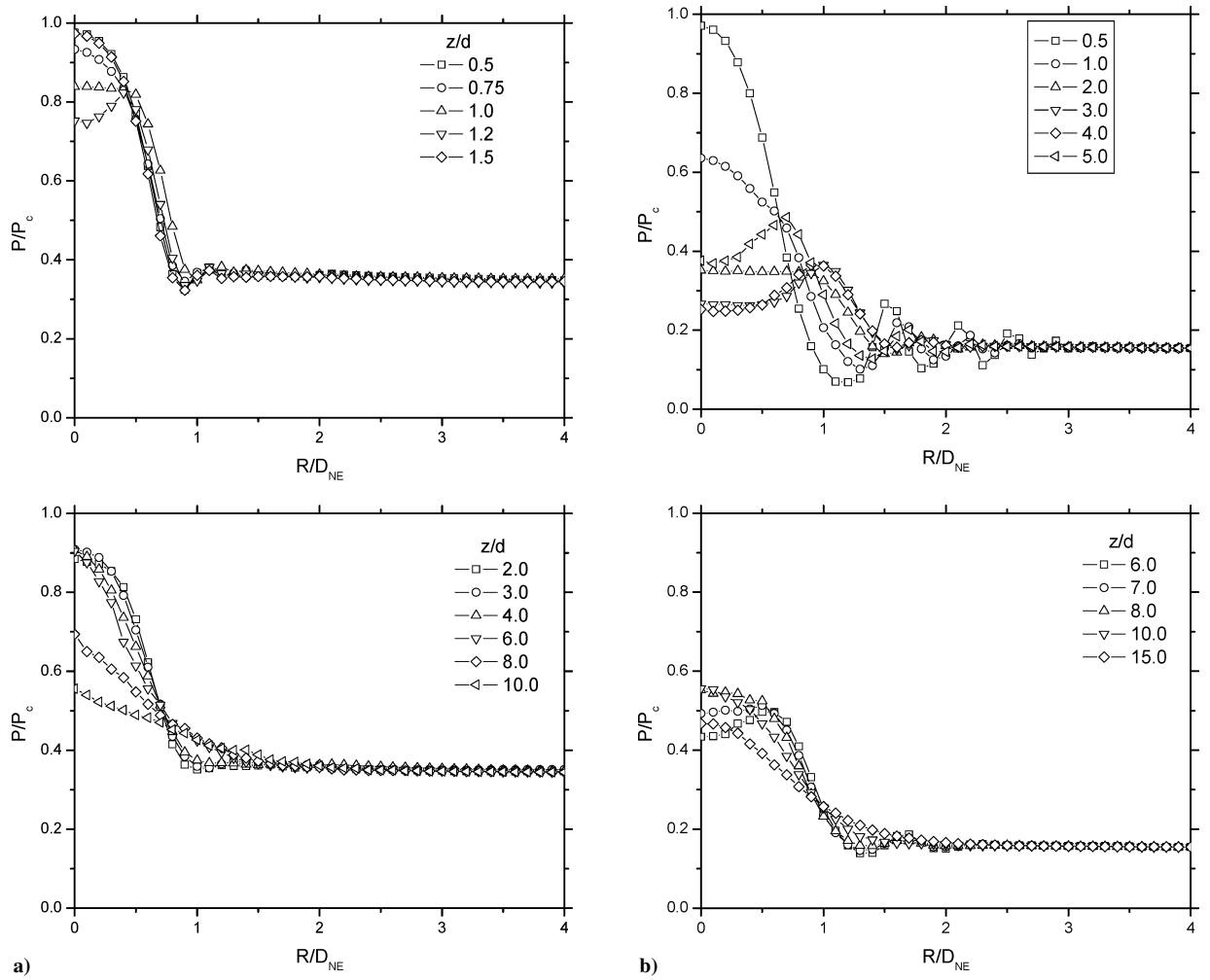

Fig. 2 Surface pressure profiles for different underexpansion ratios: a) $P_e/P_a = 1.5$ and b) $P_e/P_a = 3.5$.

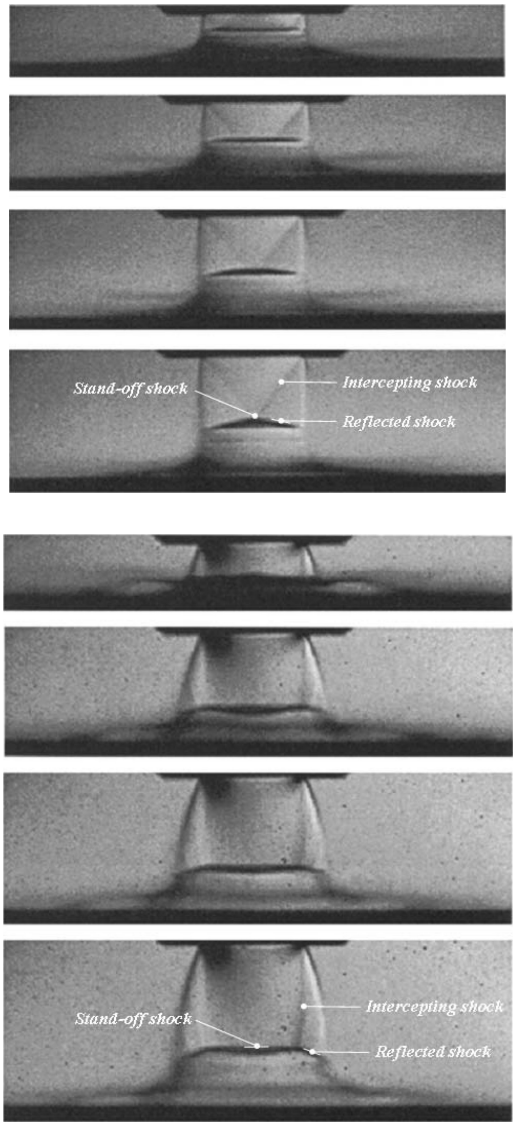

Fig. 3 Shadowgraph results for shock structure in jet: a) $P_e/P_a = 1.5$ ($Z_P/D_{NE} = 0.5$, 0.75, 1.0, and 1.2) and b) $P_e/P_a = 3.5$ ($Z_P/D_{NE} = 0.5$, 1.0, 1.25, and 1.5).

remains normal to the jet. Therefore, the jet flow passing through these two kinds of shock waves is divided into two regions. One of them is the central flow, which passes through the normal standoff shock and is decelerated to a subsonic jet. However, the outer flow, which passes through the oblique reflected shock, maintains its supersonic state due to its low pressure loss. Therefore, a shear layer is developed along the slip surface that exists between these two flows. Also, in certain cases where this pressure difference between the central and outer flow regions is very large, it may cause boundary-layer separation. As a result, the cases where the annular maximum appears in Fig. 2a imply the possibility of boundary-layer separation and the formation of the stagnation bubble.[7]

For higher underexpansion ratios (Figs. 2b), compared with the former case, the radial profiles of surface pressure show a similar tendency with increasing nozzle-to-plate distance, except at the wall jet region. In the wall jet region, the surface pressure rises and falls periodically. Its amplitude decays with increasing radial distance, and the pressure value gradually approaches the atmospheric pressure. These alternating compression and expansion regions in the wall jet are known to be produced by repeated reflections of the waves between the upper boundary of the wall jet and the plate surface.[7]

As the nozzle-to-plate distance increases over the initial expansion length, significant pressure recovery occurs at the central region. This pressure recovery is supposed to occur due to the inward momentum diffusion from the outer region where the pressure is relatively high. For $P_e/P_a = 1.5$ (Fig. 2a), the pressure profile has a central maximum when the impinging plate is positioned just downstream of the initial expansion length ($Z_P/D_{NE} = 1.25$). This steep pressure recovery can be explained by the small size of the standoff shock for the plate position near the initial expansion length ($Z_P/D_{NE} = 1.2$) in Fig. 3a. This small size of the standoff shock creates a small central region behind it, and the momentum diffusion can easily affect the entire central region, resulting in a steep pressure recovery. However, for a higher underexpansion ratio (Fig. 2b), an annular maximum persists even though the nozzle-to-plate distance is larger than the initial expansion length ($Z_P/D_{NE} = 3.7$) because the inward momentum diffusion can not easily affect a large subsonic core behind the central standoff shock.

B. Heat Transfer Coefficient

The variations of Nusselt number Nu_0 on a stagnation point with increasing nozzle-to-plate distances are presented for two different underexpansion ratios in Fig. 4. The surface shows a larger heat transfer effect on a stagnation point in most of nozzle-to-plate distances when it is impinged on by a highly underexpanded jet. However, at very short nozzle-to-plate distances, there are some points

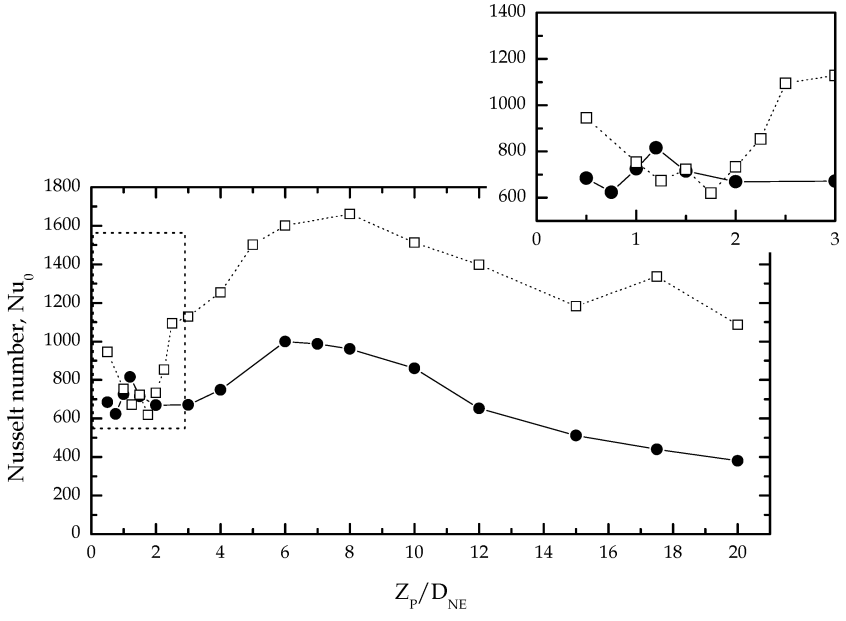

Fig. 4 Stagnation Nusselt number distribution for different underexpansion ratios: ●, P_e/P_a = 1.5 and □, P_e/P_a = 3.5.

where this phenomenon is not satisfied ($1.0 < Z_P/D_{NE} < 2.0$). This is supposed to be related to the fact that the momentum loss at the standoff shock is higher in a highly underexpanded jet than in a moderately underexpanded jet. As the nozzle-to-plate distance increases, the diffusion effect of turbulent shear flow and the fast convection speed along the surface come to surpass this momentum loss, showing high heat transfer coefficients for the highly underexpaned case.

Figure 5 presents the comparison of this result with surface pressure variation on a center point. For the underexpansion ratio of 1.5 (Fig. 5a), the stagnation Nusselt number distribution has two maximum values at $Z_P/D_{NE} = 1.2$ and 6.0. As mentioned in the Introduction section, only one peak is known to appear in a stagnation Nusselt number distribution for the case of a subsonic impinging jet. Therefore, this Nusselt number distribution showing two peaks is the characteristic of a supersonic impinging jet, which includes a shock structure. In this case, the initial increase and decrease of the stagnation Nusselt number seem to appear because the turbulence level changes depending on the distance between a standoff shock and an impinged surface. This phenomenon can be explained as follows. As the nozzle-to-plate distance increases, the distance between a standoff shock and an impinging surface also increases in a close nozzle-to-plate range. As long as this detached distance of a standoff shock from a surface is short enough ($Z_P/D_{NE} < 1.2$), the heat transfer on a central region increases with an increasing distance due to the turbulence diffusion effect into a jet core. However, if the detached distance of a standoff shock exceeds this range, the radial turbulence diffusion reduces the maximum turbulence level in a central region, resulting in a decrease of heat transfer on the stagnation point. Another rise and fall of the stagnation Nusselt number appear around a secondary peak at $Z_P/D_{NE} = 6.0$. It is believed that the secondary increase and decrease are related to the turbulence diffusion from a jet edge, as in the case of subsonic impinging jet. In particular, when the nozzle-to-plate distance increases over the secondary peak position, the stagnation Nusselt number decreases monotonically because the overall jet momentum decreases as much as the turbulence level.

For the case of a highly underexpanded jet (Fig. 5b), the stagnation Nusselt number distribution has an additional peak at the nozzle-to-plate distance of 1.5. This peak seems to be related to the increased turbulence by the interaction between a standoff shock and a jet shock occurring due to a flaw in the nozzle inner surface. When the turbulence diffuses into the central region from the slip surface, the stagnation Nusselt number increases with increasing nozzle-to-plate distance as in the moderately underexpanded case. In this region ($Z_P/D_{NE} = 1.75$ and $Z_P/D_{NE} = 8.0$), the stagnation surface pressure also increases due to the entrainment of a high-pressure flow from outside a slip surface, although it perturbs a little during the pressure recovery. This perturbation is observed because additional shock structures are generated weakly but repeatedly behind an initial strong shock cell, and each shock structure causes the small pressure loss and recovery. When the nozzle-to-plate distance

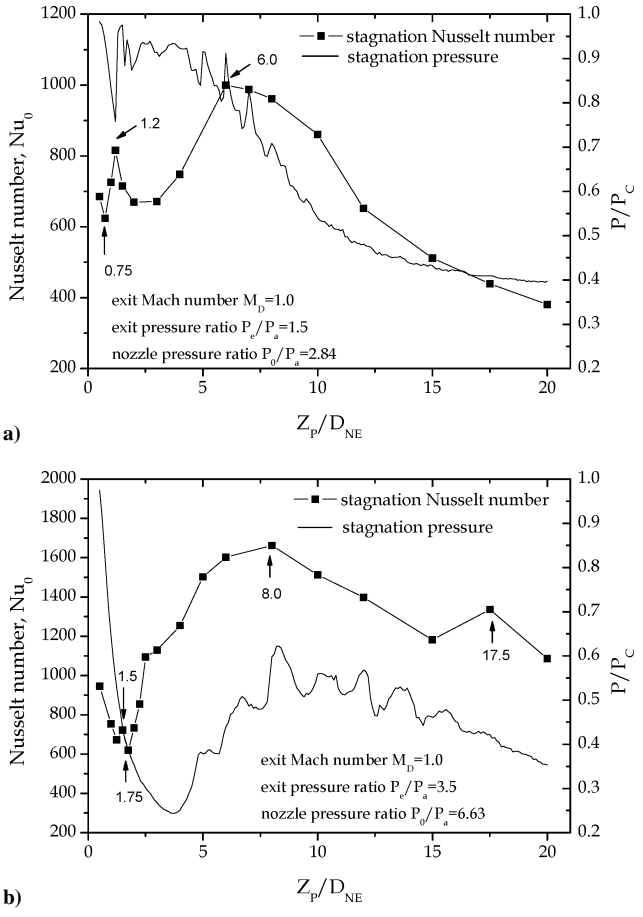

Fig. 5 Stagnation Nusselt number and stagnation pressure distributions: a) P_e/P_a = 1.5 and b) P_e/P_a = 3.5.

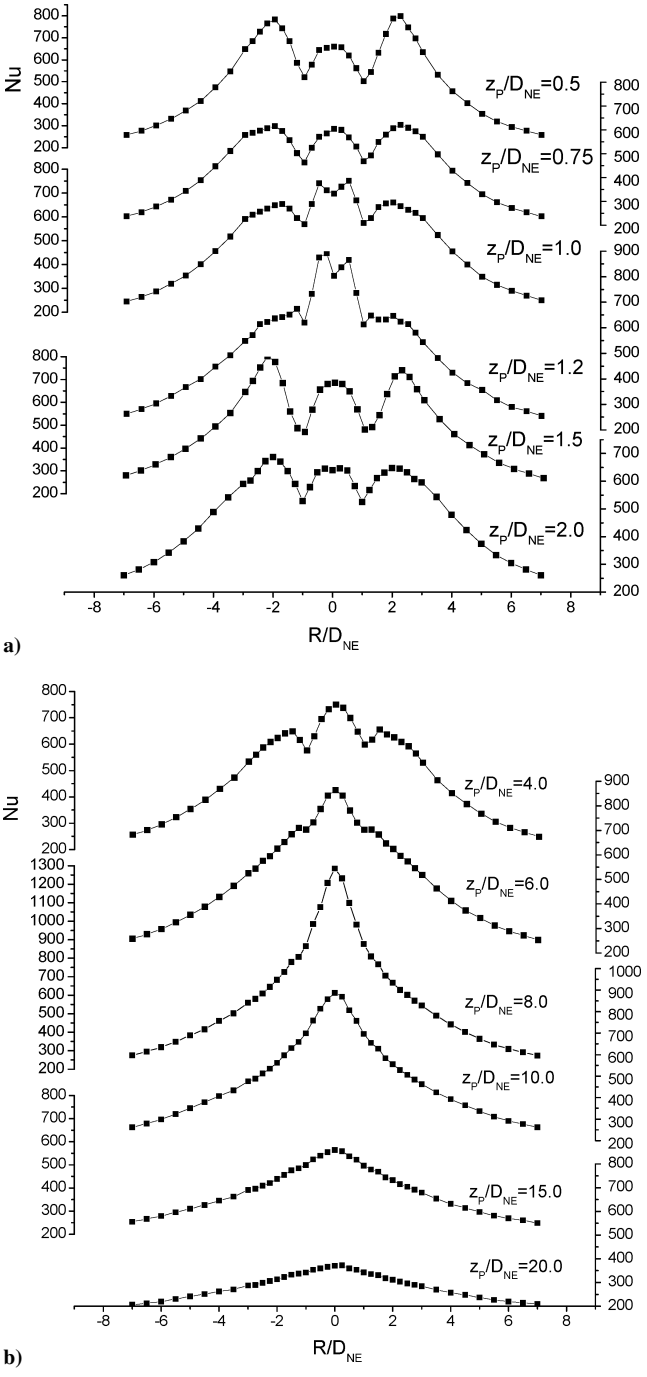

Fig. 6 Nusselt number distribution for P_e/P_a = 1.5: a) $0.5 \le Z_P/D_{NE} \le 2.0$ and b) $4.0 \le Z_P/D_{NE} \le 20.0$.

increases over this position ($Z_P/D_{NE} = 8.0$), the Nusselt number decreases together with the stagnation surface pressure in a downward direction. Another peak of the stagnation Nusselt number appears around $Z_P/D_{NE} = 17.5$. The same reason for the moderately underexpanded case explains this heat transfer variation, that is, the diffusion of turbulence that is generated at the jet edge affects this phenomenon.

The variations of Nusselt number in a lateral direction are presented in Figs. 6–9 for different underexpansion ratios. The profile has very complex variations depending on the nozzle-to-plate distance. For the underexpansion ratio of 1.5 (Fig. 6), at close distances from the nozzle exit, the Nusselt number has a peak at the center point and another annular peak at $R/D_{NE} \approx \pm 2$. Compared with the surface pressure distribution at the same nozzle-to-plate distance, it is found that no annular peak appears at $R/D_{NE} \approx \pm 2$ (Fig. 8a). According to the explanations from previous investigators,[2,3,11] the appearance of the annular peaks seems to be related to the increased turbulence caused by boundary-layer transition or the growth of secondary vortex rings along the surface in the wall jet region. As

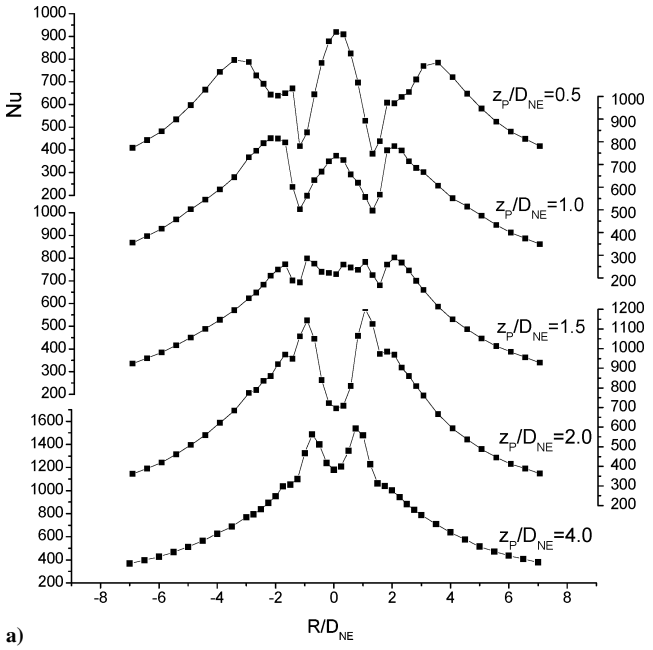

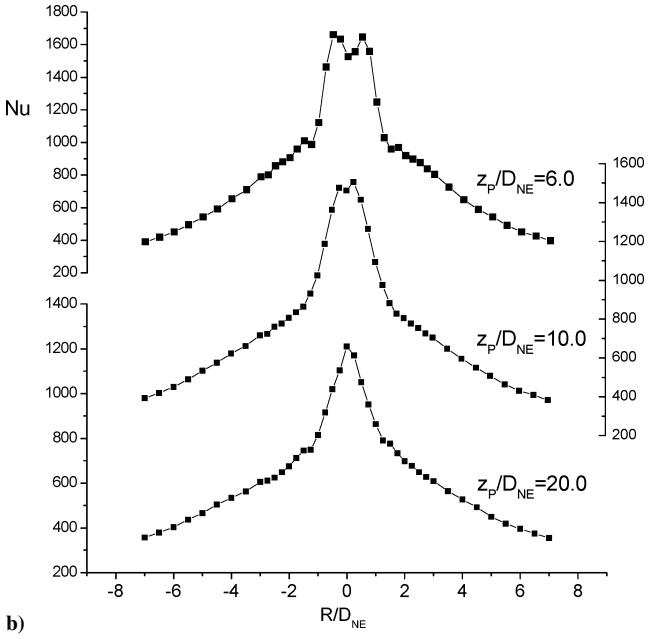

Fig. 7 Nusselt number distribution for P_e/P_a = 3.5: a) $0.5 \le Z_P/D_{NE} \le 4.0$ and b) $6.0 \le Z_P/D_{NE} \le 20.0$.

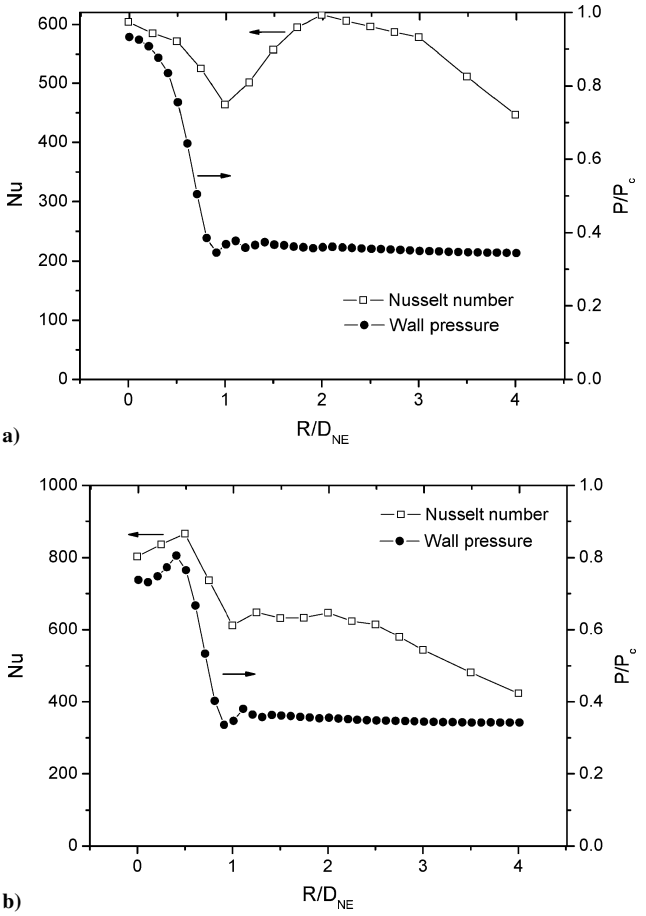

Fig. 8 Comparison of radial Nusselt number distribution with wall pressure (P_e/P_a = 1.5): a) Z_P/D_{NE} = 0.75 and b) Z_P/D_{NE} = 1.2.

the nozzle-to-plate distance increases, the central peak disappears, showing an additional annular peak at $R/D_{NE} \approx \pm 0.5$. This variation can be observed at $Z_P/D_{NE} = 1.2$ in Fig. 8b, and the annular peak of surface pressure is also observed at a similar radial position. This annular peak of surface pressure appears due to the existence of a stagnation bubble in the central region, and this recirculation zone is divided from the outer flow zone by a slip surface. Therefore, at the radial position where the slip surface and the impinged surface meet, the high surface pressure appears. Also, at this position, the high heat transfer characteristic appears due to the effect of high turbulent shear flow around a slip surface. As the nozzle-to-plate distance increases, the momentum diffusion into the jet core induces the shear layer at a slip surface to disappear, resulting in a reduction of the overall Nusselt number at a central region, whereas the surface pressure increases due to the disappearance of a stagnation bubble (Fig. 2). When the impinging plate is positioned farther downstream, the radial position where the outer annular peak appears comes close to the center point because the freejet becomes a fully turbulent flow because of the turbulence diffusion from the jet edge. Beyond $Z_P/D_{NE} = 10.0$, the Nusselt number variation has a simple bell shape, showing a maximum at the stagnation point and declining smoothly in the radial direction.

When the underexpansion ratio is increased up to $P_e/P_a = 3.5$ (Fig. 7), general trends in variation are similar to those for $P_e/P_a = 1.5$. However, the heat transfer is affected significantly by the turbulence diffusion from the sonic surface rather than $P_e/P_a = 1.5$. The Nusselt number is high at the inner annular region, whereas the heat transfer in the central region is very low due to the isolation of low-speed flow behind the standoff shock. Also, the overall heat transfer coefficients are higher than that of the moderately underexpanded jet ($P_e/P_a = 1.5$) because the transport speed of jet flow is much higher at $P_e/P_a = 3.5$. When the surface pressure and the Nusselt number variations are compared, as shown in Fig. 9, it is found that the radial position of annular peak

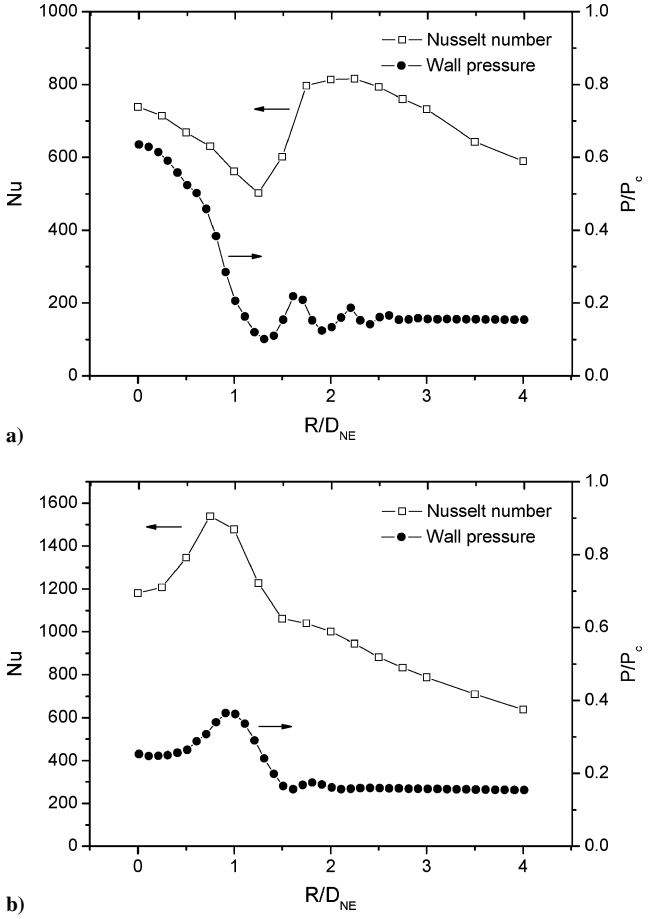

Fig. 9 Comparison of radial Nusselt number distribution with wall pressure (P_e/P_a = 3.5): a) Z_P/D_{NE} = 1.0 and b) Z_P/D_{NE} = 4.0.

coincides roughly with that for the surface pressure at $R/D_{NE} \approx 1.0$ for $Z_p/D_{NE} = 4.0$ (Fig. 9b). This phenomenon is not observed in a short nozzle-to-plate distance ($Z_P/D_{NE} = 1.0$), where the shear layer around a slip surface is not developed enough to improve the heat transfer on an impinged surface (Fig. 9a).

VI. Conclusions

An experimental investigation was conducted to examine heat transfer characteristics on a flat surface impinged by an axisymmetric underexpanded sonic jet. From the surface pressure variation, the annular peak appears in a central region, implying the existence of a stagnation bubble in it. For a highly underexpanded jet, this stagnation bubble remains until a large nozzle-to-plate distance is reached, even though the plate is positioned over the initial expansion length. From the shock visualization results, it is believed that the large size of the standoff shock is related to this maintenance of a stagnation bubble. The Nusselt number variation shows that the annular peak appears in a central region when the stagnation bubble is supposed to exist. This high heat transfer characteristic appears because the shear flow developed along a slip surface improves the heat transfer in an annular region, where the shear flow meets the impinged surface. This is considered a unique phenomenon of a high-speed impinging jet, which has a shock structure in it. Also, like the subsonic impinging jet, the lateral variation of Nusselt number shows that a high heat transfer appears at $R/D_{NE} \approx \pm 2.0$ due to the wall jet flow transition to turbulent flow or to the flow separation by secondary vortex movement. Finally, from the investigation on the effect of an underexpansion ratio, it is found that the maximum Nusselt number at stagnation point for $P_e/P_a = 3.5$ is roughly two times larger than that for $P_e/P_a = 1.5$.

Acknowledgments

This research was supported by the Agency for Defense Development and by the Ministry of Science and Technology through their National Research Laboratory program.

References

[1]Jambunathan, K., Lai, E., Moss, M. A., and Button, B. L., "A Review of Heat Transfer Data for Single Circular Jet Impingement," *International Journal of Heat and Fluid Flow*, Vol. 13, No. 2, 1992, pp. 106–115.

[2]Gardon, R., and Akfirat, J. C., "The Role of Turbulence in Determining the Heat Transfer Characteristics of Impinging Jets," *International Journal of Heat and Mass Transfer*, Vol. 8, No. 10, 1965, pp. 1261–1272.

[3]Gardon, R., and Cobonpue, J., "Heat Transfer Between a Flat Plate and Jets of Air Impinging on It," *International Developments in Heat Transfer*, American Society of Mechanical Engineers, New York, 1962, pp. 454–460.

[4]Pamadi, B. N., and Belov, I. A., "A Note on the Heat Transfer Characteristics of Circular Impinging Jet," *International Journal of Heat and Mass Transfer*, Vol. 23, No. 6, 1980, pp. 783–787.

[5]Gubanova, O. I., Lucev, V. G., and Plastina, L. N., "Central Breakaway Zone with Interaction Between a Supersonic Underexpanded Jet and a Barrier," *Fluid Dynamics*, Vol. 6, 1973, pp. 298–301.

[6]Kalghatgi, G. T., and Hunt, B. L., "The Occurrence of Stagnation Bubbles in Supersonic Impingement Flows," *Aeronautical Quarterly*, Vol. 27, No. 3, 1976, pp. 169–185.

[7]Ginzburg, I. P., Semiletenko, B. G., Terpigorev, V. S., and Uskov, V. N., "Some Singularities of Supersonic Underexpanded Jet Interaction with a Plane Obstacle," *Journal of Engineering Physics*, Vol. 19, 1973, pp. 1081–1084.

[8]Carling, J. C., and Hunt, B. L., "The Near Wall Jet of a Normally Impinging, Uniform, Axisymmetric, Supersonic Jet," *Journal of Fluid Mechanics*, Vol. 66, Pt. 1, 1974, pp. 159–176.

[9]Iwamoto, J., "Impingement of Under-expanded Jets on a Flat Plate," *Journal of Fluids Engineering*, Vol. 112, No. 2, 1990, pp. 179–184.

[10]Tam, C. K. W., Jackson, J. A., and Seiner, J. M., "A Multiple-scales Model of the Shock-cell Structure of Imperfectly Expanded Supersonic Jets," *Journal of Fluid Mechanics*, Vol. 163, 1985, pp. 123–149.

[11]Goldstein, R. J., Behbahani, A. L., and Heppelmann, K. K., "Streamwise Distribution of the Recovery Factor and the Local Heat Transfer Coefficient to an Impinging Circular Air Jet," *International Journal of Heat and Mass Transfer*, 1986, Vol. 29, No. 8, pp. 1227–1235.

[12]Kim, B. G., Yu, M. S., and Cho, H. H., "Recovery Temperature Measurement of Underexpanded Sonic Jets Impinging on a Flat Plate," *Journal of Thermophysics and Heat Transfer*, Vol. 17, No. 3, 2003, pp. 313–319.

[13]Kline, S. J., and McClintock, F. A., "Describing Uncertainties in Single Sample Experiments," *Mechanical Engineering*, Vol. 75, No. 1, 1953, pp. 3–8.

[14]Kline, S. J., "The Purposes of Uncertainty Analysis," *Journal of Fluids Engineering*, Vol. 107, June 1985, pp. 153–160.